Electronic, structural, and optical properties of the host and Cr-doped cadmium thioindate

C. Tablero

Citation: J. Appl. Phys. **112**, 093108 (2012); doi: 10.1063/1.4764339
View online: http://dx.doi.org/10.1063/1.4764339
View Table of Contents: http://jap.aip.org/resource/1/JAPIAU/v112/i9
Published by the American Institute of Physics.

Electronic, structural, and optical properties of the host and Cr-doped cadmium thioindate

C. Tablero
Instituto de Energía Solar, E.T.S.I. de Telecomunicación, Universidad Politécnica de Madrid, Ciudad Universitaria s/n, 28040 Madrid, Spain

(Received 13 July 2012; accepted 12 October 2012; published online 7 November 2012)

The cadmium thioindate spinel $CdIn_2S_4$ semiconductor has potential applications for optoelectronic devices. We present a theoretical study of the structural and optoelectronic properties of the host and of the Cr-doped ternary spinel. For the host spinel, we analyze the direct or indirect character of the energy bandgap, the change of the energy bandgap with the anion displacement parameter and with the site cation distribution, and the optical properties. The main effect of the Cr doping is the creation of an intermediate band within the energy bandgap. The character and the occupation of this band are analyzed for two substitutions: Cr by In and Cr by Cd. This band permits more channels for the photon absorption. The optical properties are obtained and analyzed. The absorption coefficients are decomposed into contributions from the different absorption channels and from the inter- and intra-atomic components. © *2012 American Institute of Physics*. [http://dx.doi.org/10.1063/1.4764339]

I. INTRODUCTION

The ternary semiconductor materials have recently attracted attention for a wide range of potential applications in device technology due to the presence of three different chemical components, which could allow the tailoring of some physical properties. Among these compounds, spinels comprise an important class of ceramic compounds with a variety of interesting physical properties. In particular, $CdIn_2S_4$ is an attractive material with a potential capability for applications in luminescent,[1] photoelectric,[2] x ray dosimetric property photoconductors,[3] solar cells, and light emitting diodes (LED).[4–8]

This compound is also considered a promising candidate for intermediate-band (IB) materials because its bandgap is near optimum for the implementation of an IB material.[9] An IB solar cell has an absorption layer that is characterized by the existence of a partially filled IB within the intrinsic bandgap, which is split into two sub-bandgaps. Because this IB is partially filled, it has the ability to both accept electrons from the valence band (VB) and to supply electrons to the conduction band (CB) by photoexcitation. Consequently, in addition to the electron-hole pairs generated by intrinsic VB-CB absorption, mobile holes, and electrons are generated in the VB-IB and IB-CB transitions at energies lower than the bandgap host semiconductor energy bandgap, resulting in higher photoelectric conversion efficiency.

The $CdIn_2S_4$ compound crystallizes in a spinel lattice (Figure 1). The primitive unit cell contains 2 formula units and has a lattice constant of $a = 10.797$ Å,[10–12] where the anion displacement parameter u is 0.386. Spinels have the general formula AB_2X_4, where A and B are di- and trivalent cations, respectively. In this lattice structure, there are tetrahedral and octahedral sites partially filled with group-II and group-III cations. This lattice is characterized by two structural parameters: the cubic lattice constant a and the anion displacement parameter u. The nearest-neighbor tetrahedral bond length r_t and the nearest-neighbor octahedral bond length r_o are given by $r_t = a\sqrt{3}(u - 0.25)$ and $r_o = a\sqrt{(u - 0.625)^2 + 2(u - 0.375)^2}$, respectively. At $u = 0.3875$, the two bond lengths are equal, and when $u = 3/8 = 0.375$, the anions form a perfect fcc sublattice. When u increases, the tetrahedral bond lengths increase while the octahedral bond lengths decrease.

In order to represent the site cationic distribution, it is useful to use the notation $(A_{1-x}B_x)[A_xB_{2-x}]X_4$ $(0 \leq x \leq 1)$, where the square brackets (parentheses) indicate atoms in the octahedral (tetrahedral) sites. The normal spinel structure corresponds to $x = 0$, and the inverse to $x = 1$. In a normal spinel, the A atom has four nearest-neighbor X atoms, while the B atom is at the corner of the octahedron cluster with six nearest-neighbor X atoms. The X atoms have one A atom and three B atoms as their nearest neighbors. In an inverse spinel structure, the tetrahedral sites are occupied by B atoms while the octahedral sites are occupied by equal numbers of A and B atoms.

Because of the potential of the $CdIn_2S_4$ for device applications, it is opportune to analyze its electro-optical properties. In this work, we shall present a detailed theoretical study of $CdIn_2S_4$ ternary spinel compound and of the Cr doped-spinel. With the latter, we pretend to explore the modification of the optoelectronic properties of the host spinel in order to apply these materials to optoelectronic devices. We give a quantitative discussion of the relative stability and energy bandgaps of ordered and disordered phase. Attention is also paid to the optoelectronic properties, among which we report the dielectric imaginary function and the absorption coefficients, comparing with experimental results in the literature. In particular, we analyzed the intra- and inter-atomic contributions to the optical properties. Finally, Sec. IV contains our conclusions.

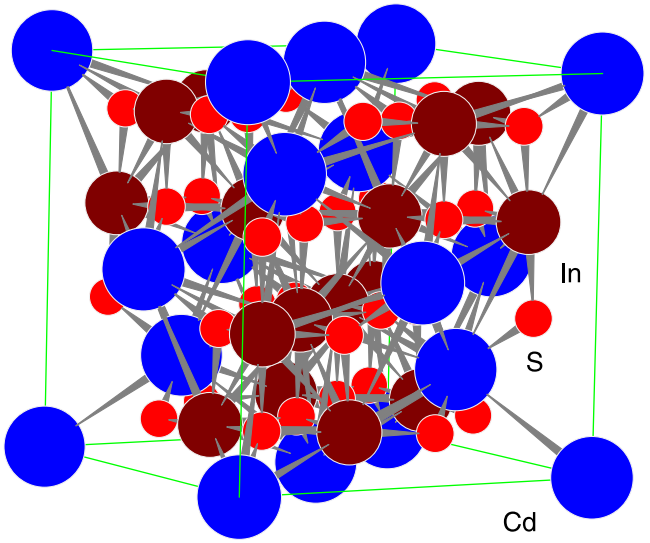

FIG. 1. Spinel lattice structure.

II. CALCULATIONS

In order to obtain the total energies, we have used the density-functional theory (DFT).[13] The standard Kohn–Sham (KS)[14] equations are solved self-consistently.[15] For the exchange and correlation term, the local-spin density approximation (LDA) has been used with the Perdew-Zunger parametrization to the Ceperley-Alder numerical data,[16] and the Generalized Gradient Approximation (GGA) in the form of Perdew, Burke, and Ernzerhof.[17] The standard Troullier–Martins[18] pseudopotential is adopted and expressed in the Kleinman–Bylander[19] factorization. The KS orbitals are represented using a linear combination of confined pseudoatomic orbitals.[20] An analysis of the basis set has been carried out using from single-zeta to triple-zeta with polarization basis sets for all atoms and by varying the number of the special k points in the irreducible Brillouin zone (BZ).

Supercells containing from 14 to 252 atoms have been used. The bigger supercells have only been used in a few cases in order to compare them with 112 atom supercells. In all of the results presented in this work, a double-zeta with polarization localized basis set has been used with periodic boundary conditions and 108, 18, and 6 special k points in the irreducible Brillouin zone for a 14-, 112-, and 252-atom cell.

To determine the optical properties, the complex dielectric function (e_2) is calculated as a function of the photon energy (E), the energy ($E_{\mu,\vec{k}}$), and occupations ($f_{\mu,\vec{k}}$) of the μ band at point $\vec{k}$ of the Brillouin zone (BZ), and the momentum matrix elements:

$$e_2(E) \sim \frac{1}{E^2}\sum_{\vec{k}}\sum_{\mu}\sum_{\lambda}|p_{\mu\lambda}|^2[f_{\mu,\vec{k}}-f_{\lambda,\vec{k}}]\delta(E_{\lambda,\vec{k}}-E_{\mu,\vec{k}}-E). \quad (1)$$

The other optical properties are obtained using the Kramers-Kronig relations. In order to obtain e_2, the occupation factors $f_{\mu,\vec{k}}$ and the energies $E_{\mu,\vec{k}}$ are determined from the aforementioned total energy calculation. The momentum-operator optical matrix elements $p_{\mu\lambda} = \langle\mu,\vec{k}|\hat{p}|\lambda,\vec{k}\rangle$ between the states $|\mu,\vec{k}\rangle$ and $|\lambda,\vec{k}\rangle$ of the μ and the λ bands at point $\vec{k}$ of the BZ are calculated directly. To consider the overall absorption process, we need to include the occupation factors to represent the absorption process from the μ to the λ bands ($f_{\mu,\vec{k}}[1-f_{\lambda,\vec{k}}]$) and the emission process from the λ to the μ bands ($f_{\lambda,\vec{k}}[1-f_{\mu,\vec{k}}]$). Then, the occupation factors for the overall absorption-emission process are $[f_{\mu,\vec{k}}-f_{\lambda,\vec{k}}]$.

III. RESULTS AND DISCUSSION

It is generally accepted that $CdIn_2S_4$ crystallizes in a normal spinel structure. Nevertheless, studies involving partial inverse structures and mixed crystals have also been reported.[21] In the normal $CdIn_2S_4$ structure, the In atom has six nearest-neighbor S atoms at 2.58 Å, the Cd atom is surrounded by 4 S at 2.54 Å, and the S atom is bounded by 1Cd (2.54 Å) and 3In (2.58 Å).

A. Change of the gap energy with *u*

The cation distribution in the lattice spinel is characterized by the anion displacement parameter u. In order to explore how the cation distribution affects the electronic structure, we have analyzed the energy gaps with u for different lattice parameters. The results are shown in Figure 2. The maximum gap for the normal structure ($x=0$) corresponds with $a=10.77$ Å and $u=0.388$. These values are next to the experimental: $a=10.797$ Å and $u=0.386$.[10–12] The energy difference between the maximum energy gap and the energy gap calculated for the experimental parameters ($E_g=2.00$ eV) is lower than 0.01 eV, which is similar to the calculation precision. In order to analyze the energy gap with the supercell size, we have obtained this gap using the experimental parameters for all supercells used (from 14 to 252 atoms). In all cases, the energy gap is 2.00 ± 0.01 eV. The energy gap for the inverse structure ($x=1$) doesn't present any maximum; it is always lower than the normal structure. The energy difference among the lattice parameters

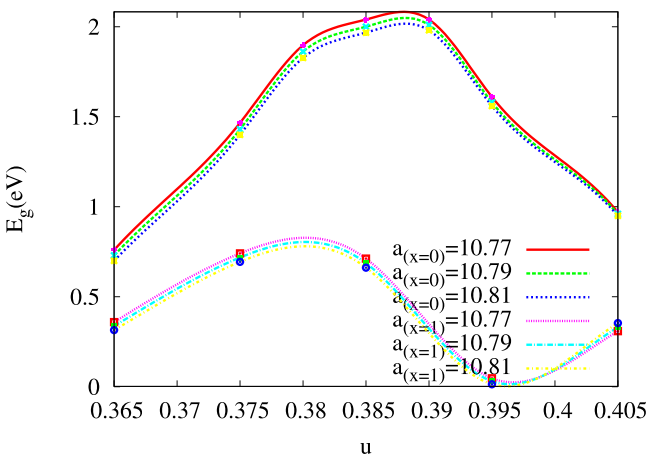

FIG. 2. Energy gap versus anion displacement parameter u for the normal ($x=0$) and inverse ($x=1$) structures for different lattice parameters (Å).

analyzed around the experimental value is similar to the calculation error.

The bandgap for the inverse spinels is smaller than those of the normal spinels because the local symmetry is reduced by the distribution of atoms in the inverse structure. This lowering of local symmetry causes further level repulsion within the VB and within the CB, pushing up the VB maximum and pushing down the CB minimum states, thus lowering the bandgap. This effect is similar to that observed in semiconductor alloys, where, due to symmetry-lowering-induced band repulsion, the alloy bandgap is smaller than the composition averaged bandgap.[22] Thus, in principle, one can control the bandgap by controlling the cation inversion parameter x.

There is general agreement that the bandgap of $CdIn_2S_4$ is indirect[11,23–25] and that the VB maximum is not at the Γ ($k=0$) point but probably along the [110] direction.[26] The values of the indirect and direct gaps are, however, somewhat inconsistent and have a wide range of values from 2.18 to 2.75 eV.[11] From our results (Figure 3), the energy gap was obtained as indirect, in agreement with predictions by other authors.[23–25] In spite of the well-known GGA-DFT gap underestimation problem,[27–30] our results compare well with the results in the literature. More accurate first-principles approaches[27–30] that avoid the band-gap problem, such as the Green function with screened interaction approximation, the hybrid functionals, the self-interaction-corrected density-functional theory, the exact exchange method, etc., are currently not practical for large supercells.

Additionally, we have analyzed the direct or indirect character of the energy bandgap with anion displacement parameter u. Figure 4 shows the results for several u values. For $u_0 \sim 0.391$, there is a transition from a direct to an indirect energy bandgap: for $u < u_0$, the gap is indirect, whereas for $u > u_0$, it is direct. From the results in the literature,[11] the indirect and direct energy bandgaps obtained experimentally using different techniques are approximately 2.27 ± 0.16 eV and 2.61 ± 0.14 eV, respectively. The difference is 0.34 ± 0.30 eV and the error oscillating between ~0 eV and ~0.6 eV. For this reason, there have been a wide range of energy gap values and discussions about the direct and indirect bandgap character in the literature, although nowadays there is general agreement that the bandgap of $CdIn_2S_4$ is indirect.[11,23–25] Observing the figure, it can be appreciated that a change of u drive to a direct-indirect bandgap transition and to a small change in the bandgap value (~0.1 eV for the u values in the figure).

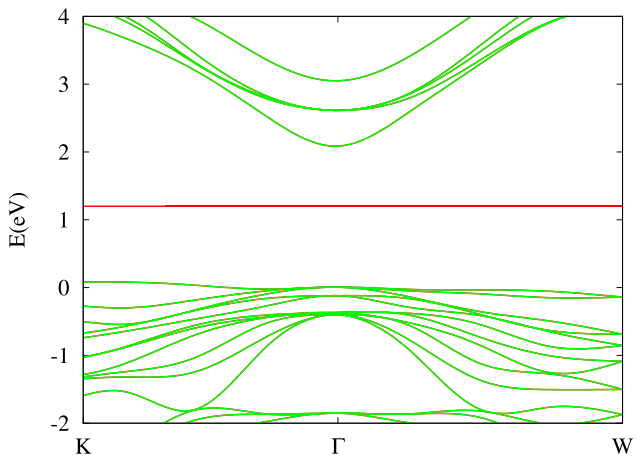

FIG. 3. Energy-band diagram of the normal structure for the K-Γ-W points in the BZ. The VB edge has been chosen as the energy origin.

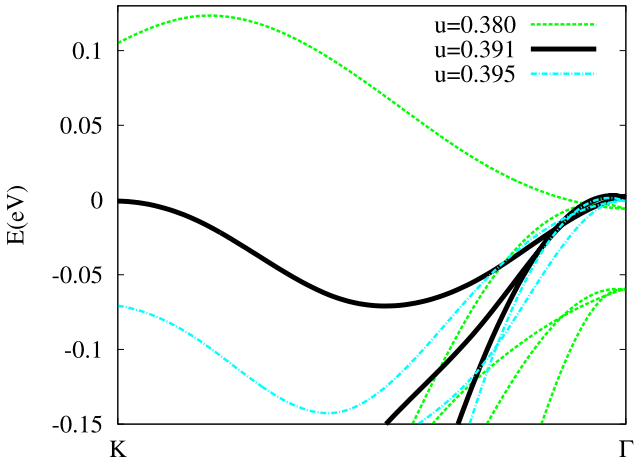

FIG. 4. Energy-band diagram between the K-Γ points in the BZ for different anion displacement parameter u. The VB edge has been chosen as the energy origin.

B. Change of the total and gap energy with *x*

For the 14-atom primitive cell, $x = 0$, 0.5, or 1 according to whether 0, 1, or 2 Cd atoms (or 4, 3, or 2 In atoms) have octahedral coordination: $(Cd_2)[In_4]S_8$ (x = 0), $(CdIn)[CdIn_3]S_8$ (x = 0.5), and $(In_2)[Cd_2In_2]S_4$ (x = 1), where the square brackets (parentheses) indicate atoms in the octahedral (tetrahedral) sites. For the normal structure, there is only one possibility for the arrangements of the atoms. However, for the completely inverse cell, there are six different degenerate arrangements of atoms on four octahedral sites. If $[A_1A_2A_3A_4]$ labels arrangements of A_i atoms on four octahedral sites, then the six different degenerate arrangements for the inverse structure are [CdCdInIn], [InCdCdIn], [InCdInCd], [CdInCdIn], [CdInInCd], and [InInCdCd]. Therefore, for x > 0, the structures are partially disordered with a lower local symmetry than the normal one.

In supercells, the simultaneous presence of different types of occupation of the tetrahedral and octahedral sites makes any value $0 \leq x \leq 1$ possible. There are many possible configurations of atoms for a given x, with the exception of the normal structure ($x = 0$), for which there is a single configuration. In order to analyze the stability and energy band gap with respect to the occupation of the octahedral and tetrahedral sites in the spinel structure, we have used a 112-atom supercell made up of 8 primitive 14-atom cells with 32 tetrahedral and 16 octahedral sites. Note that, when x is different from zero (normal structure), there are many possibilities for occupying the tetrahedral and octahedral sites. To obtain the different x values, we have combined the appropriate normal and inverse primitive cells in the supercell. This is a possibility, but there are many more for x different of zero. The results of the total energy and energy bandgap with x are shown in Figure 5. The structure

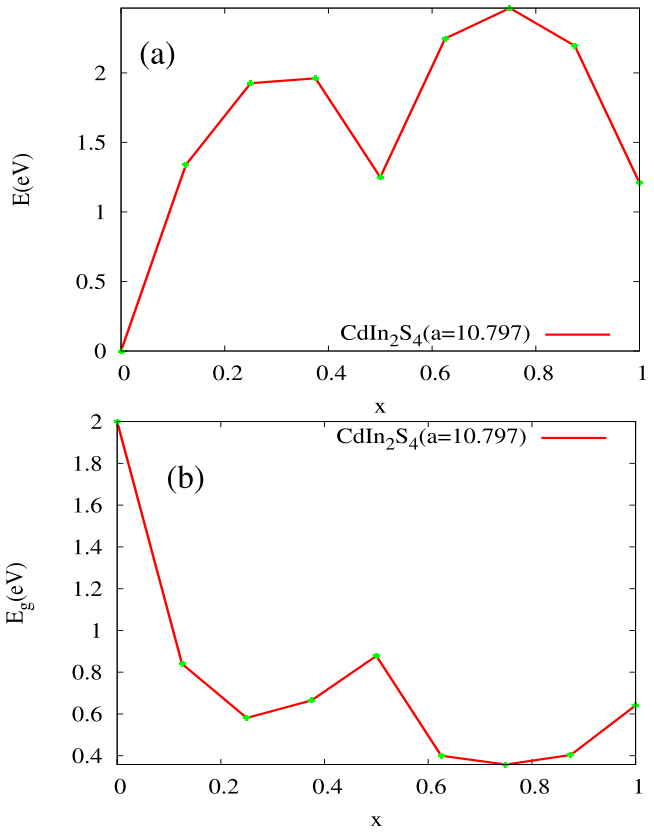

FIG. 5. Total energy (a) and energy bandgap (b) versus x for $(Cd_{1-x}In_x)[Cd_xIn_{2-x}]S_4$ using a 112-atom supercell.

with the least total energy—the more thermodynamically stable—is the normal structure (x = 0). It is in concordance with numerous results in the literature.[11,23–25] Also, the normal structure has a larger energy bandgap. This bandgap is obtained with all the supercells analyzed here, which contain 14, 56, 112, and 252 atoms. As has been aforementioned, there are many atomic configurations for a given x value, except for $x = 0$, with different total and energy gap energies. For example, for $x = 0.5$, we have analyzed two other possibilities: to make the supercell using primitive cells with $x = 0.5$, and with a combination of primitive cells (half with $x = 0$ y half with $x = 1$) distributed in different ways in the tridimensional space. The total (gap) energy of the former and latter are 1.7 eV (0.48 eV) and 3.4 eV (0 eV), larger than those shown in the figure. Fortunately, this total and bandgap energy dispersion does not affect to the normal structure, which is the more often observed experimentally. Nevertheless, this dispersion must be taken in account when results with supercells are compared for $x \neq 0$: results can be different because of the specific arrangement of atoms, although x is the same.

C. Electronic structure

For the normal structure ($x = 0$), when Cr substitutes to In (Cr_{In} substitution) the Cr atom occupies an octahedral site, whereas when it substitutes to Cd (Cr_{Cd} substitution), the Cr atom occupies a tetrahedral site. For the Cr_{Cd}or Cr_{In} substitutions, two or three of the Cr electrons are given to the bonds, thus forming an impurity level with an oxidation state +2 or +3: $Cr^{2+}(d^4)$ or $Cr^{3+}(d^3)$. The fivefold degenerate d states of Cr are split by the crystalline field into doubly degenerate d_e states with e symmetry (d_{z^2} and $d_{x^2-y^2}$) and threefold degenerate d_t states with t symmetry (d_{xy}, d_{xz}, and d_{yz}). Additionally, these states are split into spin-up (+) and spin-down (−) components. In the crystalline field with spin, the $Cr^{2+}(d^4)$ and $Cr^{3+}(d^3)$ configurations are $d^2_{e+}d^2_{t+}$ and $d^3_{t+}d^0_{e+}$. If the t and e crystal states are only formed by states of the chromium atom, then the $d^2_{e+}d^2_{t+}$ and $d^3_{t+}d^0_{e+}$ atomic configurations would correspond with the $e^2_+t^2_+$ and $t^3_+e^0_+$ configurations in the crystal.

In the (a) and (b) panels of Figure 6, the energy band structures around the Γ point in the BZ are represented. For the Cr_{In} substitution (panel a), there is an IB in the energy bandgap. This IB is empty because the Fermi energy is below this band. Also, this IB is made up by two sub-bands, indicating that it could correspond to a doubly degenerate e state. For the Cr_{Cd} substitution (panel b), the IB within the host energy bandgap is partially full (the Fermi energy is within this band) and it is made up by three sub-bands similar to the triply degenerate t state. The total number of electrons in this IB is two, indicating that it is partially full.

The crystal wavefunctions with t symmetry are formed by the combination of the d_t and by the states with the t symmetry of the host (h_t): $t^{(i)} \simeq \alpha_i \cdot d_t + \beta_i \cdot h_t$. These h_t states correspond mainly to the neighboring anions' p-S states: six when the Cr atom occupies an octahedral site (Cr_{In} substitution) and four when it occupies the tetrahedral site (Cr_{Cd} substitution). This is similar for the e states. These conclusions are confirmed from projected density-of-states (DOS) analyses. Additionally, it is observed that the t_+ and e_+ crystalline states do not contribute significantly to the CB, whereas the t_- and e_- crystalline states do not contribute appreciably to the VB. Therefore, the t_+ states for the Cr_{Cd} substitution and the e_+ states for the Cr_{In} substitutions within the energy bandgap correspond with the anti-bonding combination of the d-Cr and h_t states. The bonding combination is within the VB. Because the t_+ and e_+ states also have a contribution from the host states, the $e^2_+t^2_+$ and $t^3_+e^0_+$ configurations are not the $d^2_{e+}d^2_{t+}$ and $d^3_{t+}d^0_{e+}$-Cr configurations. This fact is deduced from panels (c) and (d) in Figure 6, where the number of d_{t+} and d_{e+} states is represented as a function of energy. The total charge (in electron units) of the state is equal to the number of states for the Fermi energy.

For the Cr_{In} substitution the d_{t+} states are full, and the d_{e+} states have an occupation of ∼0.65 electrons per d_{e+} state (∼0.65 in the VB and 0 in the IB because the e_+ –IB is empty).

For the Cr_{Cd} substitution, the d_{e+} states are full, and the d_{t+} states are partially full with an occupation of ∼0.85 electrons per d_{t+} state (∼0.55 in the VB and ∼0.30 in the t_+-IB). The t_+-IB is the anti-bonding combination, whereas the bonding combination is within the energy band gap. The d_{t+}-Cr charges will correspond with $d^{3\times0.3}_{t+}$. This is different to the t^2_+ crystalline charge. The difference in the number of electrons between $d^{3\times0.3}_{t+}$ and t^2_+ for the Cr_{Cd} substitution is distributed among the h_t states, which correspond mainly to the neighboring anions' p-S states.

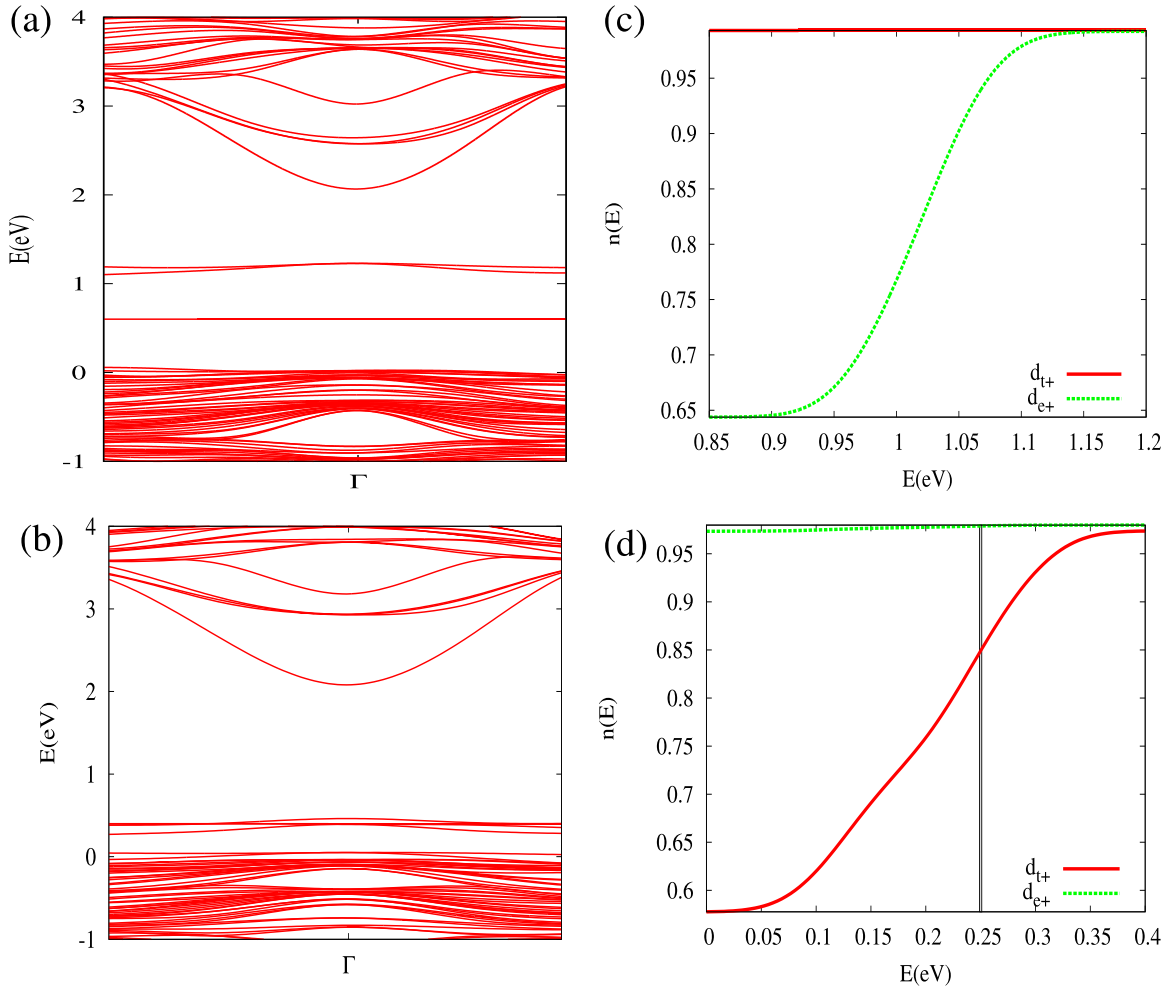

FIG. 6. Energy-band diagram for the Cr_{In} (a) and Cr_{Cd} (b) substitutions around the Γ point in the BZ. Number of d_{t+} and d_{e+} Cr states per multiplicity state degeneration (3 and 2 for d_{t+} and d_{e+}, respectively) for the Cr_{In} (c) and Cr_{Cd} (d) substitutions. The VB edge has been chosen as the energy origin. The horizontal lines in panes (a) and (b), and the vertical line in panel (d) is the Fermi energy.

D. Optical properties

Figure 7 shows the dielectric imaginary function for the normal cadmium thioindate structure obtained as aforementioned in the calculation section. In this figure, our results are compared graphically with other experimental result in the literature.[31] The difference between the results for lower energies is mainly due to the fact that the energy bandgap from the calculations (2.00 eV) is lower than the value in Ref. 31. Although we only consider the direct optical transitions, our result compares well with the experimental result despite the bandgap being indirect. This is because the difference between the direct and indirect energy bandgap is very small.

Because of the IB within the energy bandgap for the Cr doped spinel, the probability of photon absorption is larger than for the host semiconductor. For the majority spin component of the Cr_{In} substitution, in addition to the VB-CB transition, the transition from the VB to the empty *e*-IB within the energy bandgap is also possible. This is observed in panel (a) of the Figure 8, which shows the absorption coefficient decomposed into the VB-CB and VB-IB transitions. For the Cr_{Cd} substitution, because the *t*-IB within the energy bandgap is partially full, the possible transitions are VB-CB, VB-IB, IB-CB, and IB-IB. The VB-IB and IB-CB paths allow a photon with energy lower than the host semiconductor bandgap to be absorbed, increasing the mobile carriers (electrons in the CB and holes in the VB) with

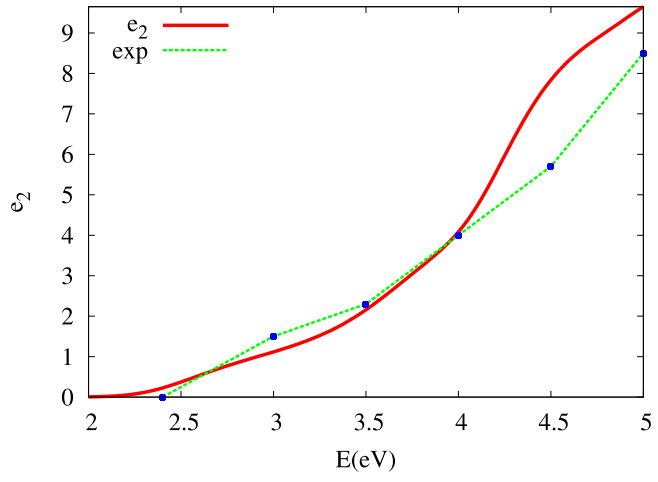

FIG. 7. Comparison of the imaginary part of dielectric constant (e_2) versus photon energy. The "exp" label corresponds with the experimental values of Ref. 31.

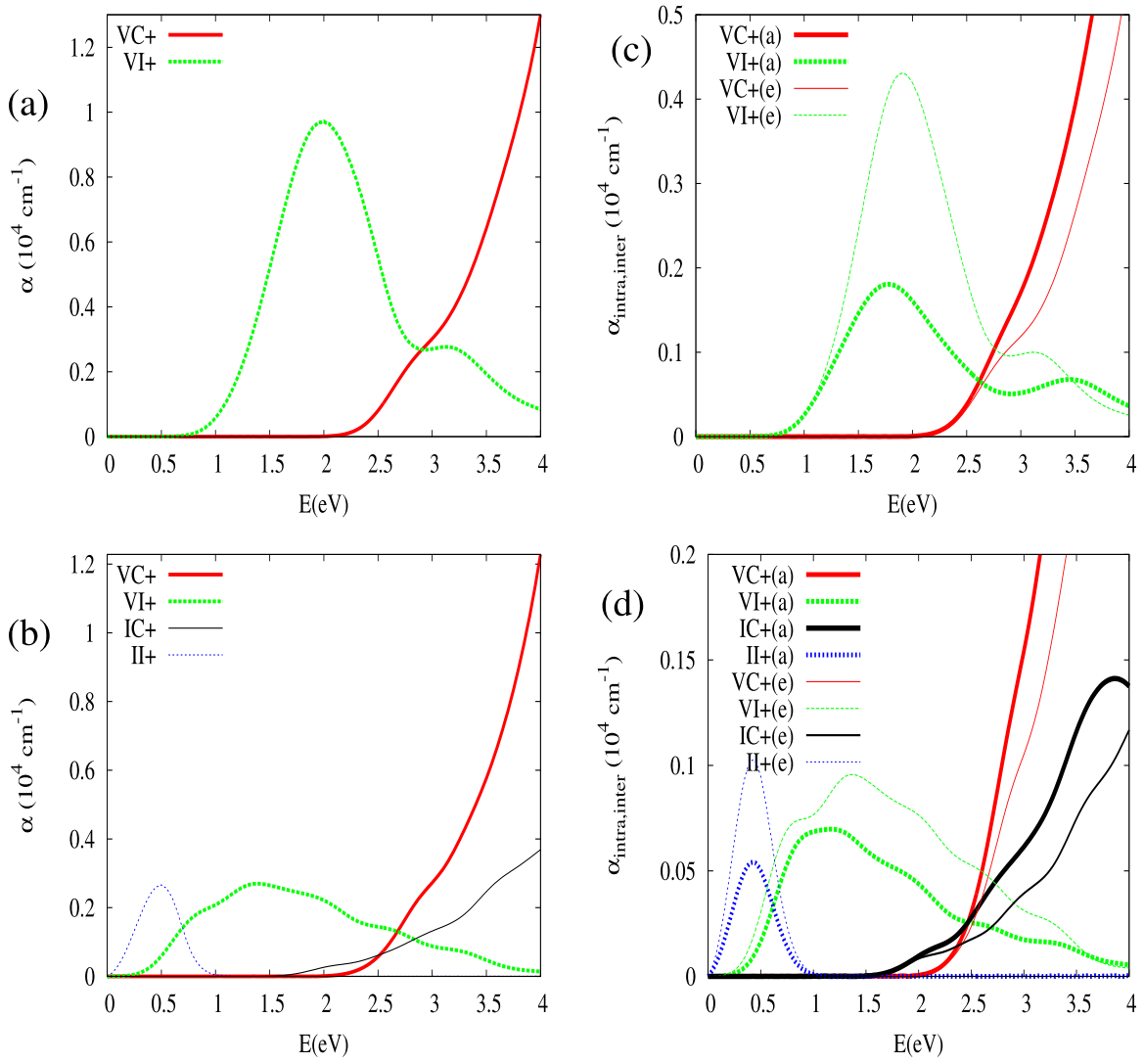

FIG. 8. Absorption coefficients $\alpha(E)$ for the majority spin component (+) of the Cr_{In} (a) and Cr_{Cd} (b) substitutions split in their components: VI+ (between VB and IB), VC+ (between VB and CB), IC+ (between IB and CB), and II+ (inside the IB). Contribution of the inter (e) and intra (a) transitions to the absorption coefficients for the majority spin component (+) of the Cr_{In} (c) and Cr_{Cd} (d).

respect to the host semiconductor. This implies a larger efficiency when these types of compounds are used to absorb the solar radiation in solar cells.

The operator matrix elements $p_{\mu\lambda}$ between the λ and μ bands can be split as $p_{\mu\lambda} = p^{(e)}_{\mu\lambda} + p^{(a)}_{\mu\lambda}$, where $p^{(a)}_{\mu\lambda}$ is the component that couples basis set functions on the same atom (intra-atomic) and $p^{(e)}_{\mu\lambda}$ is the component that couples basis set functions of different atoms (inter-atomic). The optical properties depend on the square of the momentum operator matrix elements, which can be separated into three terms: intra-atomic (depending on $|p^{(a)}_{\mu\lambda}|^2$), inter-atomic (depending on $|p^{(e)}_{\mu\lambda}|^2$), and a coupling term (depending on $|p^{(e)}_{\mu\lambda}||p^{(a)}_{\mu\lambda}|$). By performing this separation, we have obtained the intra- and inter-atomic contributions to the absorption coefficient (panels (c) and (d) in Figure 8). Both inter- and intra-atomic components are important. In particular, the inter-atomic component is large for the sub-gap energies because the IB has contributions from the impurity and host states (mainly from the anions' p-S states).

In a solar cell, with or without an IB, the external contacts are made to the VB and CB. The IB-IB transitions don't influence significantly the solar cell operation. Nevertheless, the inter-atomic contribution to the IB-IB transition (panel (d) in Figure 8) reveals that the IB has contributions from different atoms: Cr and the closer S neighbors.

IV. CONCLUSIONS

We have presented a theoretical study of the structural and electronic properties of the host and Cr-doped ternary spinel semiconductor $CdIn_2S_4$. Our results for the equilibrium lattice, internal distortion parameter u, and imaginary dielectric function for the host are in good agreement with experiment.

One of the main effects of Cr_{Cd} and Cr_{In} substitutions in the electronic structure of the $CdIn_2S_4$ host is to create an IB within the energy bandgap. For the Cr_{Cd} substitution, the IB is partially full, which could make it important for solar cell applications. For the Cr_{In} substitution, the IB is empty. The symmetry of the IB is different for the two substitutions because the local impurity symmetry is different. For both substitutions, the IB is made up of the d-Cr and p-S states of the closer Cr neighbors.

Because of the existence of the IB, there are additional photon absorption channels to those of the VB-CB host semiconductor. This fact could be used for optoelectronic devices. The Cr_{Cd} substitution could be particularly interesting for solar cells. This is reflected in the optical properties, obtained splitting the different channels. An analysis of the intra- and inter-atomic absorption components confirm that both the *d*-Cr and *p*-S states contribute to the IB, and thus, to the different absorption channels.

ACKNOWLEDGMENTS

This work has been supported by the of the National Spanish projects CONSOLIDER (CSD2006-0004), Denquiband (PLE2009-0045), Bibiana (PIB2010US-00096), and Nanogefes (ENE2009-14481-C02-01) by the European Commission through the funding of the project IBPOWER (Ref. N: Grant Agreement 211640) and NGCPV (FP7-EU-JPN 283798), and by La Comunidad de Madrid through the funding of the project NUMANCIA-2 (Ref. N: S-2009/ENE-1477).

[1]M. Springford, Proc. Phys. Soc. **82**, 1029–1037 (1963).
[2]Y. Seki, S. Endo, and T. Irie, Jpn. J. Appl. Phys. **19**, 1667–1674 (1980).
[3]S. N. Mustafaeva, M. M. Asadov, and D. T. Guseinov, Perspekt. Mater. **1**, 45–48 (2010).
[4]H. Nakanish, Jpn. J. Appl. Phys. **19**, 103 (1980).
[5]S. Endo and T. Irie, J. Phys. Chem. Solids **37**, 201 (1976).
[6]A. Anedda and E. Fortin, J. Phys. Chem. Solids **40**, 653 (1979).
[7]S. N. Baek, T. S. Jeong, C. J. Youn, K. J. Hong, J. S. Park, D. C. Shin, and Y. T. Yoo, J. Cryst. Growth **262**, 259 (2004).
[8]S. I. Radautsan, V. F. Zhitar, I. G. Kosnichan, and M. I. Shmiglyuk, Fiz. Tekh. Poluprovodn. **5**, 2240 (1971) [Sov. Phys. Semicond. **5**, 1959 (1971)].
[9]A. Luque and A. Martí, Phys. Rev. Lett. **78**, 5014 (1997).
[10]H. Hahn, G. Frank, W. Klinger, A. D. Störger, and G. Störger, Z. Anorg. Allg. Chem. **279**, 241 (1955).
[11]O. Madelung, *Semiconductors: Data Handbook* (Springer-Verlag, 2000).
[12]S. N. Mustafaeva, M. M. Asadov, and D. T. Guseinov, Inorg. Mater. **47**, 844 (2011).
[13]P. Hohenberg and W. Kohn, Phys. Rev. B **136**, B864 (1964).
[14]W. Kohn and L. J. Sham, Phys. Rev. **140**, A1133–A1138 (1965).
[15]J. M. Soler, E. Artacho, J. D. Gale, J. D, A. García, J. Junquera, P. Ordejon, and D. Sánchez-Portal, J. Phys. Condens. Matter **14**, 2745 (2002) and references therein.
[16]J. P. Perdew and A. Zunger, Phys. Rev. B **23**, 5048 (1981); D. M. Ceperley and B. J. Alder, Phys. Rev. Lett **45**, 566 (1980).
[17]J. P. Perdew, K. Burke, and M. Ernzerhof, Phys. Rev. Lett. **77**, 3865 (1996); J. P. Perdew and M. Ernzerhof, Phys. Rev. Lett. **78**, 1396 (1997).
[18]N. Troullier and J. L. Martins, Phys. Rev. B **43**, 1993 (1991).
[19]L. Kleinman and D. M. Bylander, Phys. Rev. Lett. **48**, 1425 (1982); D. M. Bylander and L. Kleinman, Phys. Rev. B **41**, 907 (1990).
[20]O. F. Sankey and D. J. Niklewski, Phys. Rev. B **40**, 3979 (1989).
[21]W. Czaja and L. Krautsbauer, Phys. Status Solidi **33**, 191 (1969); R. Brown, M. D. Martin, and W. A. Shand, J. Phys. C **3**, 1329 (1970).
[22]S.-H. Wei, L. G. Ferreira, J. E. Bernard, and A. Zunger, Phys. Rev. B **42**, 9622 (1990).
[23]F. Meloni and G. Mula, Phys. Rev. B **2**, 392 (1970).
[24]K. Y. Rajpure, V. L. Mathe, and C. H. Bhosale, Bull. Mater. Sci. **22**, 927 (1999).
[25]H. Nakanishi, S. Endo, and T. Irie, J. Phys. Colloques **36**, C3–163 (1975).
[26]A. Baldereschi, F. Meloni, F. Aymerich, and G. Mula, Inst. Phys. Conf. Ser. **35**, 193 (1977).
[27]R. M. Martin, *Electronic Structure* (Cambridge University Press, 2004).
[28]K. Ohno, K. Esfarjani, and Y. Kawazoe, *Computational Materials Science, From ab initio to Monte Carlo Methods* (Springer, 1999).
[29]R. G. Parr and W. Yang, *Density Functional Theory of Atoms and Molecules* (Oxford, New York, 1989).
[30]J. F. Dobson, G. Vignale, and M. P. Das, *Electron Density Functional Theory, Recent Progress and New Directions* (Plenum, New York, 1998).
[31]E. Grilli, P. Cappelletti, and M. Guzzi, Phys. Status Solidi (a) **50**, K93 (1978).